Full Paper

Propellants, Explosives, Pyrotechnics

DOI: 10.1002/prep.201400023

Modeling Ignition and Thermal Wave Progression in Binary Granular Pyrotechnic Compositions

Sebastian Knapp,*[a] Volker Weiser,[a] Stefan Kelzenberg,[a] and Norbert Eisenreich[a]

Dedicated to Beat Berger (1949–2014)

Abstract: Oxidizer and fuel particles are the ingredients of classical pyrotechnics. Particle concentration, size, melting, evaporation, and decomposition of the particles, heat and mass transfer, reaction kinetics, and heat of reaction control the burning behavior of these mixtures. A hot-spot approach models the reaction progress in three dimensions taking into consideration the particulate nature of pyrotechnic compositions. The governing reaction is assumed to be the oxidizer decomposition described by an Avrami-Erofeev model. Predominantly, the distribution of the oxidizer and fuel particles and their size for various concentrations influence the burning rate beneath the reaction kinetic parameters. The computational results were compared with experimental progression rates and temperatures measured for an example system composed of various Al/CuO-thermite mixtures with aluminum contents from 8% to 70%. The particle sizes were fixed to micrometer-scale. The curve of progression rate calculations depending on the aluminium particle concentration and their distribution show the same shape as the experimental results.

Keywords: Thermite reaction

1 Introduction

Typical representatives of binary particle reactions are thermite reactions. They were first described in 1898 by H. Goldschmidt as a "carbon-free" method to extract metals by reducing their oxides with aluminum [1]. Still this type of reaction is of widespread interest to rapidly produce large amounts of heat at high temperature levels and has found many applications [2]. So the thermite welding process is still the most frequently used method for welding of railroad tracks [3], it is also used to purify ores of some metals. The preparation of ceramics is also a well-known domain for thermite reactions [4]. Due to the large heat release and its self-sustaining nature, thermites have been used in warheads as incendiary devices [5]. As a big advantage most microscopic thermite compositions are not very sensitive towards friction, impact and shock.

In general, thermite reactions can be described as exothermic chemical reactions, where a metal-oxide ($M^2{}_{x2}O_{x3}$) is reduced by a less noble metal (M^1) to form the more stable metal-oxide ($M^1{}_{x4}O_{x5}$) and resulting metal (M^2). The overall reaction equation is given as [6]:

$$M^1 + \frac{x_5}{x_3 x_4} M^2_{x2} O_{x3} \rightarrow \frac{1}{x_4} M^1_{x4} O_{x5} + \frac{x_2 x_5}{x_3 x_4} M^2 \quad (1)$$

Couples of M^1 and M^2-oxides can be chosen on the basis of their position in the electrochemical series or their Gibbs energy from the Ellingham diagram of the oxidation of elements with pure oxygen [7]. Important fuels are aluminum and magnesium.

Currently, numerous investigations on thermite reactions are done using different metals and metal oxides [8] studying burning rates [9], influence of particle size [10] and pressure [11,12]. However, the physico-chemical mechanisms of thermite type reactions are still far from being completely understood. Therefore, the modeling is also of particular interest [13] and there are some preliminary approaches for it [14], which describe particle ignition and propagation of reaction fronts in porous energetic materials [15–17]. In these studies, we only used the heat flow equation with a zero order reaction and obtained the result by application of the Green's function mirrored at the boundaries. In principle, any reaction mechanism might be included. We baptized this approach Hot-Spot modeling. It is very suitable for granular systems since it contains a particle-like character by itself. This simplified model – we will discuss the model and its simplifications below – only requires reduced numerical expense and computational time. The investigations with the Hot-Spot model were not only performed to learn more about the chemical behavior but also about the influence of physical properties. Especially

[a] *S. Knapp, V. Weiser, S. Kelzenberg, N. Eisenreich*
Fraunhofer Institut für Chemische Technologie ICT
76327 Pfinztal, Germany
**e-mail: sebastian.knapp@ict.fraunhofer.de*

the influence of fuel and oxidizer densities at same particle size and thereby the number of fuel and oxidizer particles will be discussed. In this way the particle distribution and their arrangement dependent on the fuel concentration is of special interest.

For a comparison of the modeling results with a real example system a series of aluminum/copper(II)oxide thermite formulations was studied experimentally. The temperature and propagation rates at different fuel/oxide concentration ratios were determined including the necessary input parameters for the model.

2 Theory: The Hot-Spot-Model for Two-component Pyrotechnic Materials

Modeling of the ignition and combustion of an energetic material composed of fuel and oxidizer particles is difficult to achieve. In the case of a thermite reaction it is still not sufficiently explored how the reaction starts and proceeds. Depending on the melting point of the considered fuel and oxidizer and the decomposition temperature of the oxide it may happen that one or both ingredients are molten before ignition. As first chemical reaction step it can be assumed that oxygen is released during the thermal decomposition of the involved oxide. The released oxygen would diffuse outwards and react immediately with the fuel. The thermal decomposition is being considered the rate-determining step. This assumption would then nicely explain the high, thermal stability, and the high ignition energy required to set off thermites. This model assumption is not in contrast to the widely accepted picture of the aluminum oxidation starting with the melting of aluminum and fracturing of the alumina shell. These processes can be neglected because they take place before the decomposition of the oxide and release of oxygen. The oxidation reaction cannot start until both components oxygen and fuel are available. Therefore the decomposition of the oxide is the rate-determining step and used here as the starting point.

The model described herein for the reaction of thermites induces substantial simplifications with respect to the "real" process and uses the following assumptions:

(i) Oxidizer and fuel are present in separated particles of defined sizes distributed randomly or regularly according to predefined stoichiometry. On reaction they form a single homogeneous condensed material.
(ii) The oxidizer particles decompose to release oxygen due to an initial local heat pulse. The decomposition of the oxidizer is the rate-determining step.
(iii) The oxygen is distributed by diffusion (diffusion equation) to the metal component to enable a contact for the reaction.
(iv) Phase transitions are neglected.
(v) On contact fuel and oxidizer react to the final product in an overall second order reaction (this reaction is in reality very fast at the conditions of the thermite reaction), with kinetics governed by the kinetic constants of the thermal decomposition of the oxidizer.
(vi) The heat generated by the reaction is distributed according to the heat flow equation.
(vii) The transport coefficients are assumed to be independent of temperatures and species concentrations.

The main physical processes in the combustion of condensed energetic materials like pyrotechnic mixtures are heat and mass transfer. This means heat and species are generated and consumed by various processes at the combustion front and distributed in the material and the burnout zone. Transferring the hot spot model to the description of heterogeneous reactions the heat flow equation has to be solved simultaneously with the mass transfer equation. As a consequence, to model such processes, the related partial differential equations have to be solved in three dimensions for temperature and at least three species c_i:

$$\rho c_p \frac{\partial T[\vec{x},t]}{\partial t} - \lambda \cdot \Delta T[\vec{x},t] = \dot{Q}[\vec{x},t] \tag{2}$$

$$\frac{\partial c_i[\vec{x},t]}{\partial t} - D_i \Delta c_i[\vec{x},t] = \dot{c}_i[\vec{x},t] \tag{3}$$

where ρ is the density, c_p the specific heat capacity, λ the heat conductivity, D_i the diffusion coefficient for the i-th species and $c_i[\vec{x},t]$ the concentration of component i. The equations describe the propagation of the scalar temperature field and species fields in space and time in dependency of the physical properties of the material and of the source terms on the right hand side. The source terms comprised the chemical reactions, the related heat and species generation and consumption.

In the case of the combustion of pyrotechnic mixtures, the chemical reaction is exothermic and consequently a heat release occurs. The source term of the energy release by the chemical reaction is given for a general reaction scheme by:

$$\dot{Q}[\vec{x},t] = \sum_i q_i \frac{\partial c_i[\vec{x},t]}{\partial t} \tag{4}$$

where q_i are the heats of reaction. The rates of reaction are given by:

$$\frac{\partial c_i[\vec{x},t]}{\partial t} = -\sum k_{i,j} f[c_i, c_j] \tag{5}$$

with the rate constant k_{ij} is given by the Arrhenius Equation:

$$k_{i,j}[T] = Z_{i,j} e^{-\frac{E_A}{RT[\vec{x},t]}} \tag{6}$$

Here, $Z_{i,j}$ is the pre-exponential factor, R the universal gas constant, T the temperature, and E_A the activation energy. The Arrhenius Equation gives the dependence of the rate constant $k_{i,j}$ of the chemical reaction on the temperature T and the activation energy E_A.

The function $f[c_i,c_j]$ in the equation above depends on the reaction scheme to be modeled. In the case of a chemical reaction of a fuel with an oxidizer generating the heat of reaction q_{reac} like $A+B\rightarrow C$ ($i=A, B, C$) an overall second order reaction is assumed. The heat output of the chemical reaction and therefore the source term for the chemical reaction energy release in the equation of heat transfer is given by:

$$\frac{dc_A[\vec{x},t]}{dt} = -k[T]c_A[\vec{x},t]c_B[\vec{x},t] \tag{7}$$

$$\frac{dc_B[\vec{x},t]}{dt} = -k[T]c_A[\vec{x},t]c_B[\vec{x},t] \tag{8}$$

$$\frac{dc_C[\vec{x},t]}{dt} = -\frac{dc_A[\vec{x},t]}{dt} = -\frac{dc_B[\vec{x},t]}{dt} \tag{9}$$

$$\dot{Q}_{reac} = q_{reac} Z_{A,B} e^{-\frac{E_A}{RT}} c_A[\vec{x},t]c_B[\vec{x},t] \tag{10}$$

To start the combustion process of a pyrotechnic mixture it must be ignited. In the heat transfer equation a second source term on the right hand side must provide an energy input at a defined point in time and space. This is called a Hot-Spot. For example it can be described by a 3D Gaussian function at position (x_0, y_0, z_0) multiplied by a Dirac distribution in time, which ensures that it occurs only at a defined time t_0:

$$\dot{Q}_{hs}[\vec{x},t] = \frac{Q_0}{(2\pi)^{3/2}\sigma_x\sigma_y\sigma_z} \cdot e^{-\left(\frac{(x-x_0)^2}{2\sigma_x^2}+\frac{(y-y_0)^2}{2\sigma_y^2}+\frac{(z-z_0)^2}{2\sigma_z^2}\right)} \cdot \delta[t-t_0] \tag{11}$$

Including the initiating hot spot at t_0 and the heat of reaction, the equation of heat transfer results in:

$$\rho c_p \frac{\partial T[\vec{x},t]}{\partial t} - \lambda \cdot \Delta T[\vec{x},t] = \sum_n \frac{Q_0}{(2\pi)^{3/2}\sigma_x\sigma_y\sigma_z} \cdot e^{-\left(\frac{(x-x_0)^2}{2\sigma_x^2}+\frac{(y-y_0)^2}{2\sigma_y^2}+\frac{(z-z_0)^2}{2\sigma_z^2}\right)} \cdot \delta[t-t_0] + q_{reac} Z_{A,B} e^{-\frac{E_A}{RT}} c_A[\vec{x},t]c_B[\vec{x},t] \tag{12}$$

Without a chemical reaction &Qdot;$_{reac}[\vec{x'},t]$ the problem can be solved analytically. Therefore several analytical and numerical methods are known [18]. However the non-linearity of the Arrhenius term makes an analytical solution impossible. Therefore, only a numerical method can be applied. In order to avoid the current cumbersome methods of numerically solving differential equations the method of Green's function is used where a numerical integration is performed which is a faster and a more stable process and enables to involve complicated geometries generated by the reaction of the individual particles. If the appropriate Green's function for the homogeneous problem is known, it only has to be convolved with the source term of the differential equation in case of infinite space. The heat source and chemical reaction are calculated by simultaneously solving the related differential equation at the selected time steps Δt.

$$T[\vec{x},t] = \int G_U[\vec{x}-\vec{x}',t-t'] \cdot \frac{\dot{Q}[\vec{x},t]}{\rho c_p} \cdot d\vec{x}' \cdot dt' \tag{13}$$

The Green's function in infinite space for the differential equation above in three dimensions is a Gaussian-like function ($\kappa=\lambda/c_p\rho$) [18].

$$G_U[\vec{x}-\vec{x}',t-t'] = \left(\frac{1}{4\pi\kappa(t-t')}\right)^{3/2} \cdot e^{-\frac{(\vec{x}-\vec{x}')^2}{4\kappa(t-t')}} \tag{14}$$

The solution of the equation of heat transfer is than given by:

$$T(\vec{x},t) = \int_0^t \int_{-\infty}^{\infty} \frac{1}{(4\pi\kappa(t-t'))^{3/2}} \cdot e^{-\frac{(\vec{x}-\vec{x}')^2}{4\kappa(t-t')}} \cdot \left(\dot{Q}_{HS}[\vec{x}',t] + \dot{Q}_{reac}[\vec{x}',t]\right) d\vec{x}'dt \tag{15}$$

The profiles of oxidizer, fuel, and reaction product proceed in an analogue way:

$$c_i(\vec{x},t) = \int_0^t \int_{-\infty}^{\infty} \frac{1}{(4\pi D(t-t'))^{3/2}} \cdot e^{-\frac{(\vec{x}-\vec{x}')^2}{4D(t-t')}} \cdot \dot{c}_i[\vec{x}',t] d\vec{x}'dt \tag{16}$$

In Equation (15) the space integral reaches over the infinite space. According to the boundary conditions of the limited dimensions of a real sample the energy will be reflected at the boundaries of the sample (mirror sources) and the integral reaches only over the sample dimensions. In case of fast reactions and steep profiles of temperature and species, the width of G_U is small compared with the size of the included space. This means, in a numerical solution of Equation (15) the integration has to include only a small section of the total space neighboring the maximum of G_U ($G_U \neq 0$). On the other hand this prevents conservation of mass and energy. But the error can be neglected for a limited number of time steps. Without interdiffusion both components fuel and oxidizer at all positions x would develop according to the solution of Equation (5) for the proposed case of a 2nd order reaction:

$$c_A[\vec{x},t] = \frac{c_{A0} - c_{B0}}{1 - c_{B0}/c_{A0} \cdot e^{(c_{B0}-c_{A0})k\cdot t}} \quad (17)$$

$$c_B[\vec{x},t] = \frac{c_{B0} - c_{A0}}{1 - c_{A0}/c_{B0} \cdot e^{(c_{A0}-c_{B0})k\cdot t}} \quad (18)$$

$$c_C[\vec{x},t] = 1 - c_A[\vec{x},t] = 1 - c_B[\vec{x},t] \quad (19)$$

For the numerical solution of the integral Equation (15) above, the algorithm mainly consists of three steps. The first step generates initial temperature and species profiles resulting from the *n* initially given hot spots and the particles of both types A and B also approximated by 3D Gaussians:

$$T_1[\vec{x},t] = \sum_{i=1}^{n}\left(\frac{Q_0}{\rho c_p (2\pi)^{3/2}\sigma_x\sigma_y\sigma_z}\cdot e^{-\left(\frac{(x'-x_i)^2}{2\sigma_x^2}+\frac{(y'-y_i)^2}{2\sigma_y^2}+\frac{(z'-z_i)^2}{2\sigma_z^2}\right)}\right)\cdot\delta[t] \quad (20)$$

$$c_{1,A,B}[\vec{x},t] = \sum_{i=1}^{n}\left(\frac{1}{(2\pi)^{3/2}\sigma_x\sigma_y\sigma_z}\cdot e^{-\left(\frac{(x'-x_i)^2}{2\sigma_x^2}+\frac{(y'-y_i)^2}{2\sigma_y^2}+\frac{(z'-z_i)^2}{2\sigma_z^2}\right)}\right)\cdot\delta[t] \quad (21)$$

For further calculations, one Gaussian hot spot initiates the thermite; however, *n* fuel and oxidizer particles are distributed according to a plan representing the experimental configuration. The initial condition for the reaction product is $c_{1,C} = 0$.

In the second step the progress of the chemical reaction (17), (18), and (19) for a small time step Δt is calculated generating:

$$T_2(\vec{x},t) = (T_1[\vec{x},t] + \frac{q_{reac}}{\rho c_p}\cdot k[T_1[\vec{x},t]]c_{1,A}[\vec{x},t]c_{1,B}[\vec{x},t]\cdot\Delta t \quad (22)$$

and:

$$c_{2,A}[\vec{x},t] = c_{1,A}[\vec{x},t] - k[T_1[\vec{x},t]]c_{1,A}[\vec{x},t]c_{1,B}[\vec{x},t]\cdot\Delta t \quad (23)$$

$$c_{2,B}[\vec{x},t] = c_{1,B}[\vec{x},t] - k[T_1[\vec{x},t]]c_{1,A}[\vec{x},t]c_{1,B}[\vec{x},t]\cdot\Delta t \quad (24)$$

$$c_{2,C}[\vec{x},t] = c_{1,C}[\vec{x},t] + k[T_1[\vec{x},t]]c_{1,A}[\vec{x},t]c_{1,B}[\vec{x},t]\cdot\Delta t \quad (25)$$

These temperature and species profiles are assumed to be instantaneously inserted, therefore being multiplied each by the Dirac Delta function $\delta(t)$. The third step is to calculate the solution of the heat transfer equation. It calculates heat and mass diffusion for the same time step Δt by convolution of the related profiles and the Green's functions.

$$T_3[\vec{x},t] = \iint\left(\frac{1}{4\pi\kappa\Delta t}\right)^{3/2}\cdot e^{-\frac{(\vec{x}-\vec{x}')^2}{4\kappa\Delta t}}\cdot T_2[\vec{x}',t']\cdot\delta(t')\cdot dx'dy'dz'\cdot dt' \quad (26)$$

$$c_{3,i}[\vec{x},t] = \iint\left(\frac{1}{4\pi D_i\Delta t}\right)^{3/2}\cdot e^{-\frac{(\vec{x}-\vec{x}')^2}{4D_i\Delta t}}\cdot c_{2,i}[\vec{x},t']\cdot\delta(t')\cdot dx'dy'dz'\cdot dt' \quad (27)$$

The integral via d*t*′ results in the integrand itself because of the Delta function. The numerical procedure e.g. 3D Gaussian quadrature performs the spatial integral on a 3D lattice [19]. In case of steep gradients and short time intervals and correlated squares of the lattice node distances Δx^2 the Green's function is of small width and strongly reduces computing time because of reducing the integral intervals to that sections where the Green's function $G_U \neq 0$. $T_3 \rightarrow T_1$ and $c_{3,i} \rightarrow c_{1,i}$ close the loop to start now iteration with a further step according to Equation (22) by including contribution of the chemical reaction terms.

Steps 2 and 3 are repeated iteratively. Step 1 can be included as often as new hot spots occur from an external heat source, which is not the case here. Figure 1 shows a schematic view of the modeling steps.

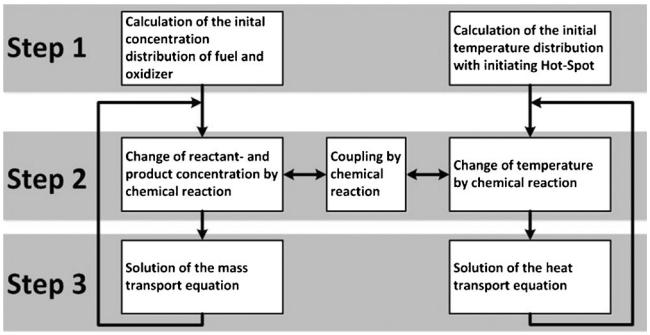

Figure 1. Schematic view of the model steps.

The calculations result in three-dimensional temperature and concentration profiles for each time step, and in heat output and position of the reaction front over time, plotted are mainly two-dimensional cross sections.

Summing up all lattice nodes after calibration where conversion is completed (e.g. for stoichiometric conditions $c_{3,A,B}[\vec{x},t] \cong 0$ or half of the conversion, maximum temperature reached) defines a conversion rate, which in linear progression can be considered as burning rate.

In pyrotechnic mixtures fuel and oxidizer particles are the sources of reacting fuel and oxidizer. Including diffusion by the same way like the heat transfer equation the particles can react, as soon as gaseous fuel and oxidizer get into contact. The model does not include any convection or radiation.

In conclusion three types of parameters are necessary to run the Hot-Spot model:

(i) Initial distributions, sizes and numbers of hot spots, fuel and oxidizer particles.

(ii) Material parameters: density, heat capacity, heat conductivity, diffusion coefficient.
(iii) Reaction parameters: heat of reaction, Arrhenius-parameters (pre-exponential factor, activation energy).

3 Experimental

3.1 Samples

Samples with different compositions of aluminium/copper(-II)oxide (Toyal Europe Alcan 400, 99.7 %min., aluminum powder atomized; Alpha Aesar Copper(II)oxide ACS, 99.0 %min., powder CuO) were milled using an automatic mortar. The stoichiometries of the compositions and the particle diameters are summarized in Table 1. A wide range of stoichiometry was realized. The particle size was determined using a laser diffraction device (Malvern Instruments Mastersizer 2000) reaching from 2 μm to 30 μm for both types of particles with mean diameters (d_{50}) of 6 μm (Al) and 9 μm (CuO). So the particles of the two components can be regarded to have the same order of size. Figure 2 exhibits SEM images of characteristic particles (Zeiss-SEM Supra 55 VP, Carl Zeiss SMT AG, Germany).

3.2 Burning Rate Measurement Setup

The experiments were performed in a nitrogen atmosphere in a chimney-type window bomb under constant pressure of 0.1 MPa N_2. To measure the progression rate 2 g of the sample mixture were filled into a test tube (Rotilabo® test tube, beaded rim, borosilic glass 5.1, thin walled, 2 mL, 70 mm long, inner diameter of 6 mm). By tapping, an initial bulk density of about 1 g cm^{-3} was produced. Ignition was performed using a melting wire enhanced with a pellet of pyrotechnic igniter compound.

The visible flame front was observed with a high-speed video camera (Redlake Motion Pro X3) using 1000 fps and a spatial picture resolution of 9 pixels mm^{-1}. From the records, the flame propagation was derived using a software code called AVICOR developed at Fraunhofer ICT for analyzing video samples of combustion processes [21]. Additionally, a macro lens was available to produce movies of 5000 fps with a limited field of view of 2×6 mm^2.

3.3 Temperature Measurement Setup

By using test tubes a problem occurs when condensed material covers the inner wall of the glass tube immediately behind the reaction front. So the tube got opaque and only emission from the colder tube wall was detected by the spectrometer. Therefore, temperatures were measured in free air on bulk material combustion. The bulk material was placed in a row of about 40 mm length and 10 mm width on a SCHOTT CERAN® plate in air. The igniter was placed at one end and obscured in a way that it did not interfere with optical measurements. For temperature measurement NIR spectra from 1.0 μm to 2.2 μm were measured using an MCS 611 PGS-NIR 2.2 spectrometer from Carl Zeiss AG, Germany equipped with an optical fibre. The spectra were calibrated using a black body radiator in intensity per unit wavelength. The fibre optics of the Zeiss spectrometers used in the experiments make a calibration in units of spectral radiance difficult. The spectra were analyzed with ICT-BaM code.

Table 1. Composition of investigated mixtures.

Material	Concentration [ma%]										
Al (Alcan 400)	5	8	13	19	24	30	40	50	55	63	70
CuO (Alfa Aesar 325mesh)	95	92	87	81	76	70	60	50	45	37	30
Mass equivalence ratio Ø	0.22	0.37	0.64	1	1.35	1.83	2.84	4.26	5.21	7.26	9.95
	Superstoichiometric (fuel lean)			Stoichiometric.	Substoichiometric (fuel rich)						

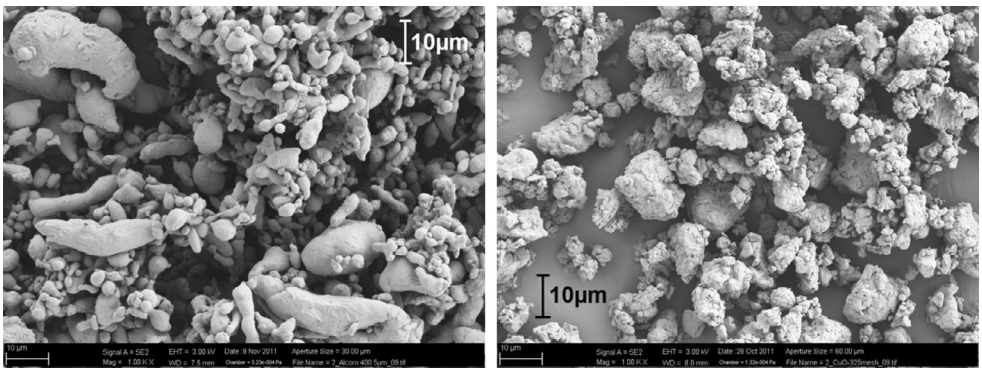

Figure 2. SEM pictures of aluminum (left) and copper(II)oxide (right) particles.

ICT-BaM does not require spectral radiance to derive temperatures from NIR because it models spectra of gaseous reaction products, soot and continuum radiation based on their band shapes. The evaluation procedure is based on a Least Squares Fit of calculated spectra to the measured ones. It is described in more detail in Ref. [22]. For the recent application only the model of grey-body emitter was needed which shows an excellent agreement between experimental and calculated spectra to determine temperature of the emitting particles. The analysis resulted in intensity, emission temperature and a signal proportional to the emissivity with a temporal resolution up to 70 Hz.

3.4 Thermogravimetric Measurement Setup

For the determination of the chemical reaction kinetic parameters, a thermogravimetric measurement of copper particles with the same particle size as the copper(II)oxide particles in the burning experiment were performed. The copper particles were used to study the oxidation process and the following spit-off of oxygen. The thermogravimetric analysis (TG) and differential scanning calorimetry (DSC) were carried out simultaneously with a heating rate of 10 K min^{-1} (Netzsch STA 449C Jupiter, Netzsch GmbH & Co. KG, Selb, Germany) in synthetic air atmosphere.

4 Results

4.1 Burning Rate

The burning experiments with test tubes result in linear progression rates. Figure 3 shows screen shots of the reaction zone at different mixture ratios.

Resulting values for the different mixtures are plotted in Figure 4 on logarithmic scale as a function of aluminum content (open circles). The values correspond to the right axis of ordinates. Although the reproducibility of the single measurements is weak, clear trends can be observed. It is well known, that the progression rate of particle mixtures depends not only on mixture ratio, particle size, temperature and pressure but also on the experimental conditions like orientation of the flame front, diameter of the speci-

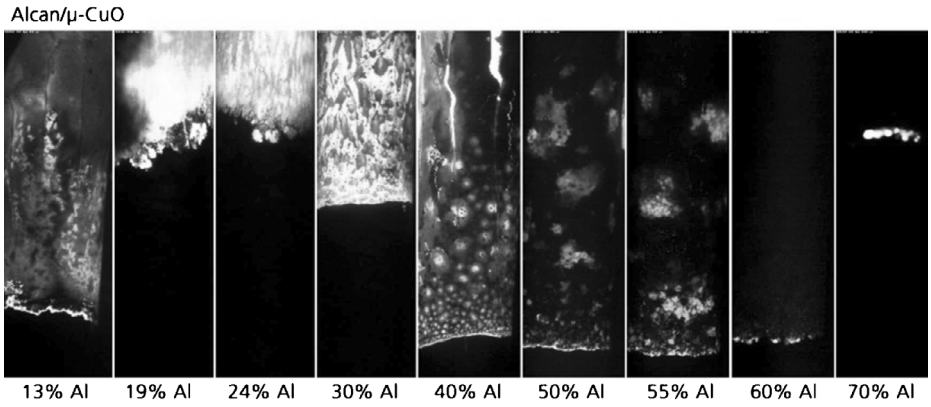

Figure 3. Screen shots of the reaction zone at different mixture ratios.

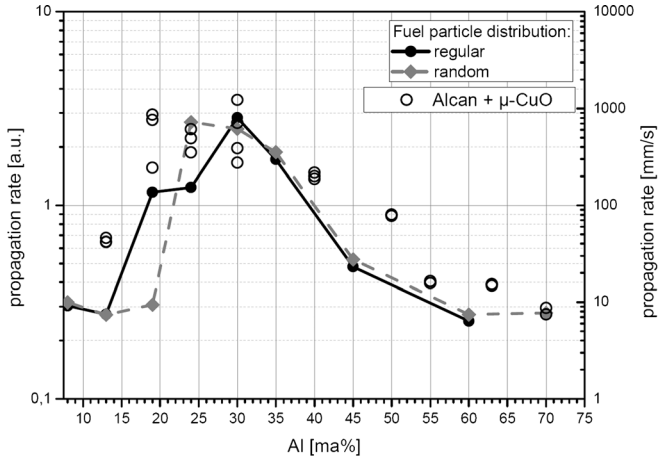

Figure 4. Modeled (left axis) and measured (right axis) propagation rates of Al/CuO thermite in dependency of the fuel concentration.

men, bulk density etc. During the recent experiments all of these parameters were held constant, so that the relations can be compared.

The progression velocity varies by more than one order of magnitude from 50 mm s^{-1} at fuel-lean conditions ($<$ 19 ma% Al) to 1000 mm s^{-1} at about stoichiometric conditions and decreases to 10 mm s^{-1} at fuel-rich conditions ($\gg$ 30 ma% Al). The highest progression rate is found near stoichiometric conditions in the substoichiometric field at 30 ma% Al.

4.2 Temperature of the Reaction Front

In Figure 5 the triangles indicate the adiabatic flame temperatures calculated with EKVI-Code [20] at 0.1 MPa. The maximum temperature, 2800 K, is close to stoichiometric ratio of 19 ma% Al. But also from 16 % to 50 % temperatures higher than 2500 K are expected. Beyond this range adiabatic temperatures decrease rapidly. Between 28–50 ma% aluminum the combustion temperature is determined by the dissociation temperature of Al_2O_3 and hence yields a plateau. Beyond 50 ma% Al the exothermicity falls and hence the temperature drops.

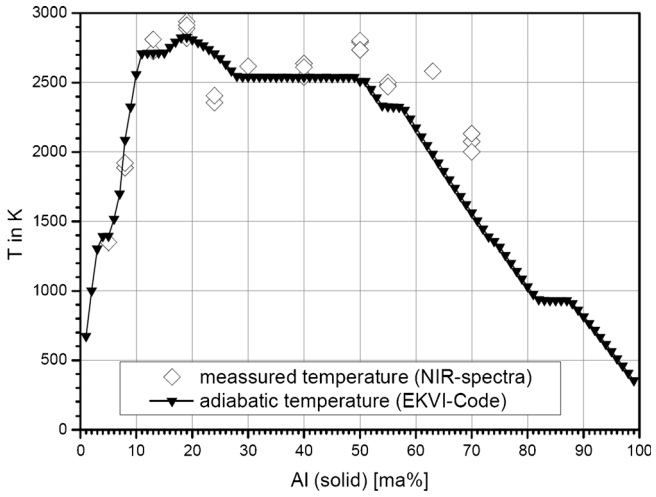

Figure 5. Calculated adiabatic temperatures and measured temperatures in dependency of fuel (aluminum) concentration.

The experimentally determined temperature values were also charted in Figure 5 as open diamonds. The absolute values are in a good agreement with the adiabatic flame temperatures calculated with EKVI-Code for the fuel lean compositions. Especially the dependence on fuel concentration corresponds well with these theoretical values. However at fuel rich conditions ($>$ 30 % Al) measured values are significantly higher than the theoretical ones. In this range, the progression velocity and with it the reaction rate is relative low so entrained air might also burn with excess aluminum. In the fuel-lean area the effect of ambient air is negligible. However in the fuel-rich area the aluminum would also react with the air oxygen and the temperature could be higher than the calculated adiabatic temperature.

4.3 Thermogravimetric Results

The Arrhenius-Parameters were determined by thermogravimetric analysis of copper in air. Under the assumption that the decomposition of copper oxide determines the speed of reaction the obtained data are used for parameter determination. The TG, DTG, and DSC curves for copper at a heating rate of $\beta = 10$ K min^{-1} are shown in Figure 6 which contains already CuO and Cu_2O. A two-step oxidation between 523 K and 650 K of copper leads to the copper oxide. At a temperature of 1280 K the copper oxide

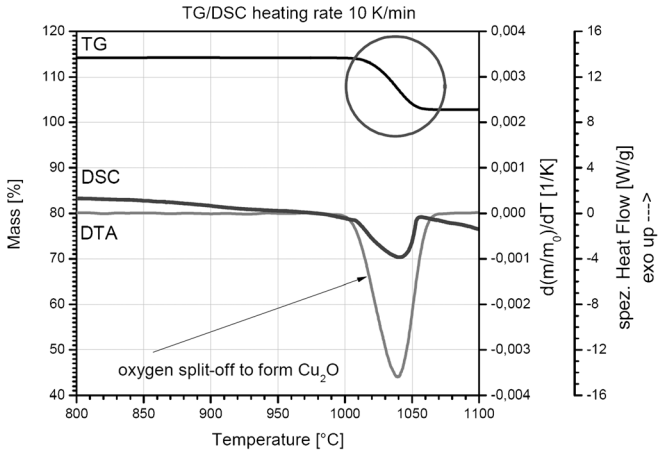

Figure 6. Example of a thermal gravimetric measurement of copper in air.

begins to split-off oxygen till a temperature of 1340 K, according to the reaction scheme:

$$2CuO \rightarrow Cu_2O + O$$

5 Modelling Results

To start the calculations with the Hot-Spot model the necessary input parameters must be defined. Therefore, first of all the number of fuel particles dependent on total number of particles, fuel concentration, particles densities and particles size was calculated as follows:

$$n_{Fuel} = \frac{n_{Tot}}{(1 - c_{Fuel}) \cdot c_{Fuel}} \cdot \left(\frac{\rho_{Fuel}}{\rho_{Oxid}}\right) \cdot \left(\left(\frac{d_{Fuel}}{d_{Oxid}}\right)^3 + 1\right) \quad (28)$$

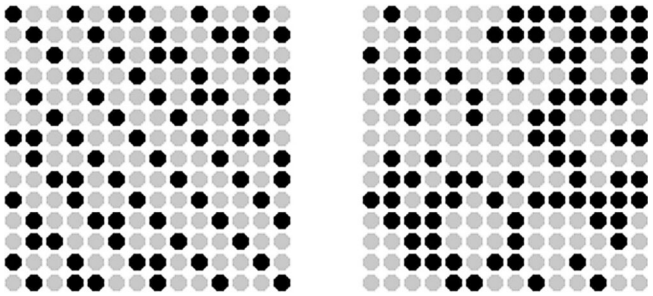

Figure 7. Particle distributions calculated for a fuel concentration of 24 mass-% and same particle size of fuel and oxidizer particles. At the left-hand side a regular distribution is shown and at the right-hand side a random distribution.

Table 2. Material parameters of fuel (aluminium) and oxidizer (copper oxide) particles found in literature [23].

Parameter	Fuel [Al]	Oxidizer [CuO]
Density ρ [g cm^{-3}]	2.7	6.48
Heat capacity c_p [J kg^{-1} K^{-1}]	897	63.68
Heat conductivity λ [W m^{-1} K^{-1}]	237	27

And the number of oxidizer particles by:

$$n_{Oxid} = n_{Tot} - n_{Fuel} \quad (29)$$

where n_{Tot} is the total number of particles, n_x the number of particles, c_x the concentration, ρ_x the density, and d_x the diameter of particle of type x (x = fuel or oxidizer). The total number of particles was fixed to 196. Fuel and oxidizer densities are from the literature (see Table 2). The particle size was experimentally determined and in a first approximation a diameter of 10 μm was chosen for both types.

The particle distribution was calculated by two different ways: a regular and a random method. The two different distributions are shown in Figure 7.

Last but not least the reaction parameters are necessary for the model. Due to the fact that the measured temperatures in the fuel-lean area are in good agreement with the adiabatic temperatures, the heat of reaction for each fuel concentration was determined from the adiabatic temperatures of the EKVI-Code calculations (Figure 5).

To determine the Arrhenius-Parameters, pre-exponential factor and activation energy, a 3rd order Avrami-Erofeev mechanism was fitted to the experimental thermal gravi-

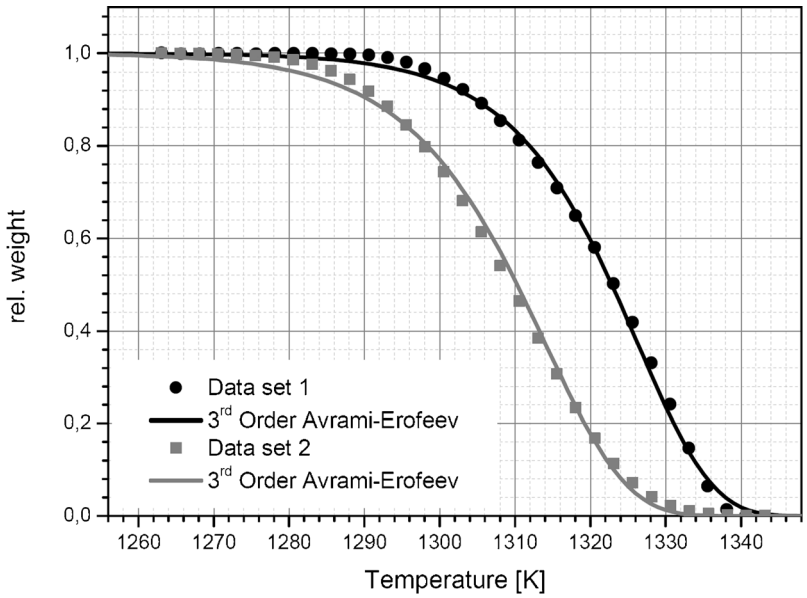

Figure 8. Simultaneous non-linear least-squares fit of a 3rd order Avrami-Erofeev mechanism to two normalized TG curves (symbols, 5 K min^{-1} and 10 K min^{-1}) using "FindMinimum" of Mathmatica8® of WolframResearch.

metric data of the decomposition of the copper oxide. A direct least-squares fit was applied (see [24]) to the sigmoid curve normalized to 1 and 0 encircled in the diagram Figure 8, using the inverse function $\alpha(T)$ in Equation (31):

$$g(\alpha) = \left(-\ln[1-\alpha]\right)^{1/3} = \frac{Z}{\beta}\int e^{-E/RT}dT \tag{30}$$

$$\alpha(T) = e^{-\left(\frac{Z}{\beta}\int e^{-E/RT}dT\right)^3} \tag{31}$$

Two thermogravimetric measurements of copper were done and the curve of the oxygen split-off analyzed by a non-linear least-squares fit (Figure 8) [24]. The results are shown in Table 3 in comparison to literature values [25]. They are in good agreement with each other and the

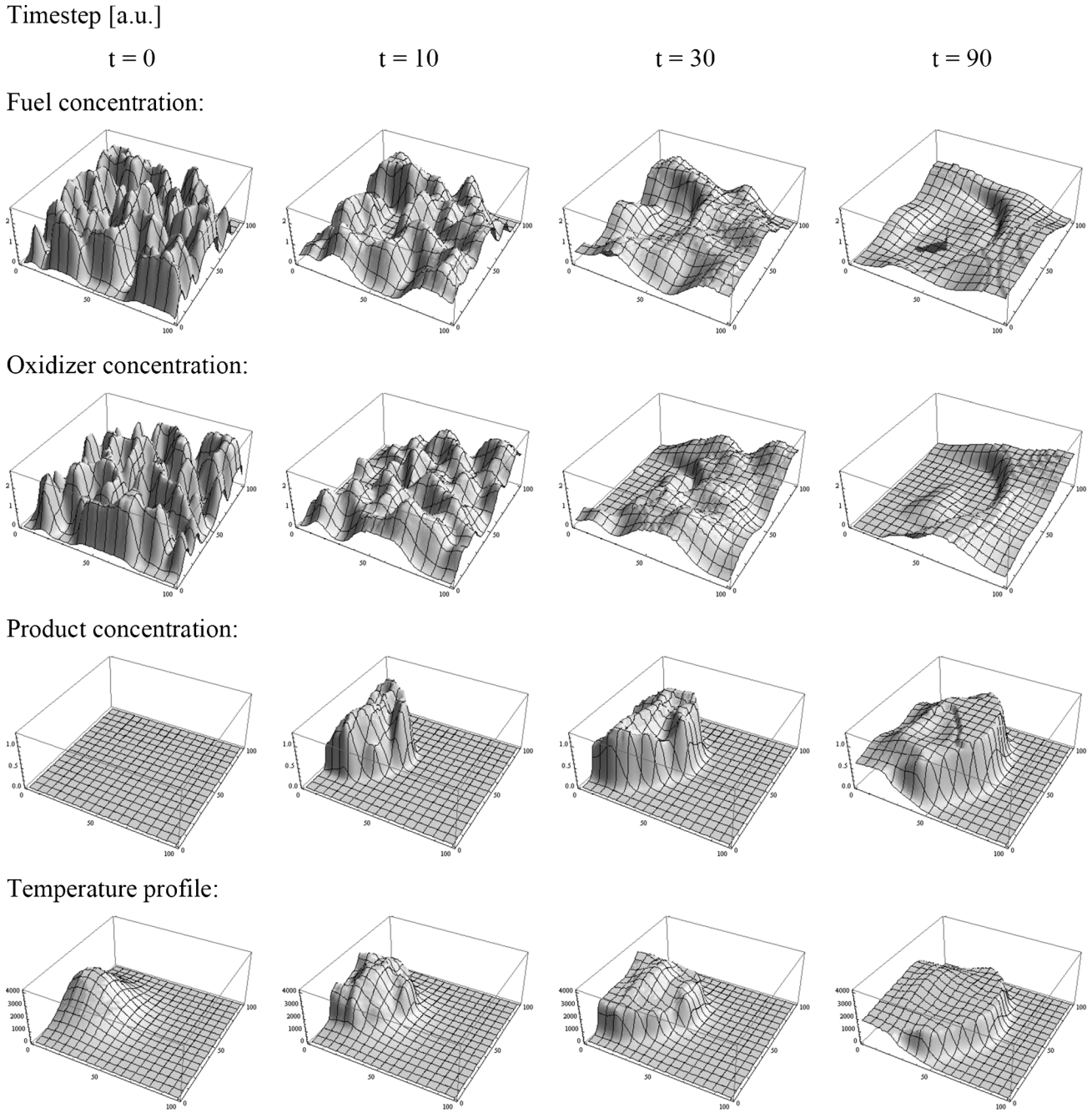

Figure 9. Fuel, oxidizer, product concentration, and temperature profile calculated by the Hot-Spot model for a random particle distribution with 30 ma% initial fuel concentration. The space units are arbitrary. The concentration reach from 0 to 1 and the temperature from 0 to 4000 K.

Table 3. Obtained Arrhenius-Parameters by fitting thermal gravimetric analysis data with a 3rd order Avrami-Erofeev model in comparison with literature values [25].

Data set	Z [s^{-1}]	E_a [K]
1	$10^{14.75}$	51539
2	$10^{16.58}$	57494
Literature	$10^{13.3}$	31994.23 (266 kJ mol^{-1})

values from dataset one were used for the Hot-Spot calculations.

With these input parameters of Table 2 and Table 3 the Hot-Spot model calculations were performed with regular and random particle distributions for the same fuel concentrations as the experiments were done. Fuel and oxidizer particle size were identical. An example output of a random distribution with a fuel concentration of 30 ma% is shown in Figure 9.

In Figure 9 in the first row the fuel concentration is shown, below the oxidizer and product concentrations and in the bottom row the temperature profile. The columns show four time steps. In the first column the initial distribution is shown. The fuel and oxidizer concentrations show the Gaussian-function shaped particles. The product concentration is zero and the temperature profile shows the single Hot-Spot to ignite the particle mixture. At this geometrical point the fuel and oxidizer concentration shows ten time steps later (column two in Figure 9) decreasing concentration and in contrast increasing product concentration and temperature profile. This continues at later time steps (column three and four) and the development of product concentration and temperature is shown.

To determine the rate of combustion the output data of the Hot-Spot model were analyzed. Therefore, in the temperature profile the position of the moving temperature front was determined over time. With a linear least-square fit the propagation rate was determined. This was done for all fuel concentrations. The resulting propagation rates are shown in Figure 4. The black dots and line shows the propagation rate of the regular particle distribution. The grey diamonds and line shows the propagation rate for the random particle distribution. Both lines correspond to the left axis of ordinates.

6 Discussion and Conclusions

First of all the Hot-Spot model described herein is an attempt to investigate the influence of certain parameters on the combustion process of granular systems. As it is work in progress it cannot be expected that all the results are in perfect agreement with the example system of Al/CuO-thermite. The first aim was to reproduce the course of the propagation rates but not the absolute values. Because of the strong simplifications it is difficult to get useful estimations of the input parameters. For the kinetics model the parameters has been derived from TG/DSC measurements, which results in similar values as from the literature. Much more difficult is the situation for parameters like the heat capacity, the heat conductivity and the diffusion coefficient. In the model, they are taken temperature-independent, which is problematic for a wide temperature range. The first choice we did, aimed to get the model running. This may explain the great absolute difference between the calculated values for the propagation rates and the measured ones.

The Hot-Spot model calculations were performed at a particle size ratio of fuel to oxidizer particle of 1:1. From that data, the propagation rates in dependency of the fuel concentration were calculated and shown in Figure 4.

In comparison to the experimentally determined propagation rates the shapes of the functions are in good agreement. The modeling results show as well as the experimental data the speed maximum to be in the same substoichiometric range. Also the sharp increase in superstoichiometric range and the flatter slope in substoichiometric range are in good agreement with the experimental results. From a fuel concentration of nearly 55 ma% the propagation rates have only a poor dependency on the fuel concentration. The sharp increase in the superstoichiometric range and the difference between the regular and random particle distribution show the strong dependency of the propagation rate in this range on the fuel and oxidizer particle arrangement in space. The accordance between the regular and random particle distribution in the substoichiometric range shows that this dependency is substantially weaker in that range.

In conclusion, it was shown that the Hot-Spot model qualitatively mimics the dependency of the propagation rate on the fuel concentration. This suggests that heat and mass transfer are the main physical processes in granular reactions, like pyrotechnic mixtures. It describes also adequately that the effect of fuel and particle configuration is not negligible particularly in the superstoichiometric range.

Symbols and Abbreviations

ρ	Density [kg m^{-3}]
c_p	Specific heat capacity at constant pressure [J kg^{-1} K^{-1}]
λ	Thermal conductivity [J s^{-1} m^{-1} K^{-1}]
c_i	Concentration of the *i*-th component [mol m^{-3}]
D_i	Diffusion coefficient for the *i*-th component [m^2 s^{-1}]
q_i	Heat of reaction [J mol^{-1}]
Z_{ij}	Pre-exponential factor [s^{-1}]
E_A	Activation energy [J mol^{-1}]
R	Gas constant [J mol^{-1} K^{-1}]
Q_0	Energy of a Hot-Spot [J]
$\dot{Q}$	Heat flow [J m^{-3} s$^{-1]}$]
T	Temperature [K]
k_{ij}	Rate constant [s^{-1}]

$\dot{Q}_{real}$ Heat flow of the chemical reaction [J s^{-1}]
$\dot{Q}_{HS}$ Heat flow of a Hot-Spot [J s^{-1}]

Acknowledgments

The authors feel grateful to intensive and fruitful discussions with Beat Berger (formerly armasuisse) who promoted these topics for decades.

References

[1] Th. Goldschmidt, *Verfahren zur Herstellung von Metallen oder Metalloiden oder Legierungen derselben*, Patent DE 96317, March 13, **1895**.
[2] L. L. Wang, Z. A. Munir, Y. M. Maximov, Review: Thermite Reactions: their Utilization in the Synthesis and Processing of Materials, *J. Mater. Sci.* **1993**, *28*, 3693–3708.
[3] C. P. Lonsdale, Thermite Rail Welding: History, Process Developments, Current Practices And Outlook For The 21st Century, Conrail Technical Services Laboratory Altoona, PA USA.
[4] O. Odawara, J. Ikeuch, Vacuum Centrifugal-Thermite Process for Producing Ceramic-Lined Pipes, *J. Am. Ceram. Soc.* **1986**, *69*, 141 C-854-86.
[5] V. Weiser, E. Roth, S. Kelzenberg, W. Eckl, Pyrotechnic Incendiaries to Combat Toxic Clouds, *40th International Annual Conference of ICT*, Karlsruhe, Germany, June 24–26, **2009**, pp. 13(1–12).
[6] V. Weiser, E. Roth, A. Raab, A. Koleczko, S. Kelzenberg, B. Berger, B. Haas, Spectroscopic Investigations on Thermite Reactions, *38th International Annual Conference of ICT*, Karlsruhe, Germany, June 26–29, **2007**, pp. 93-(1–13).
[7] H. J. T. Ellingham, Reducibility of Oxides and Sulfides in Metallurgical Process, *J. Soc. Chem. Indust.* **1944**, *63*, 125.
[8] D. Meerov, D. Ivanov, K. Monogarov, N. Muravyev, A. Pivkina, Y. Frolov, Mechanical Activation of Al/MoO3 Thermite as a Component of Energetic Condensed Systems to Increase Its Efficiency, *Cent. Eur. J. Energ. Mater.* **2009**, *6*, 277–289.
[9] K. Ilunga, O. del Fabbro, L. Yapi, W. W. Focke, The Effect of Si–Bi2O3 on the lignition of the Al–CuO Thermite, *Powder Technol.* **2011**, *205*, 97–102.
[10] M. L. Pantoya, J. J. Granier, Combustion Behavior of Highly Energetic Thermites: Nano vs. Micron Composites, *Propellants Explos. Pyrotech.* **2005**, *30*, 53–62.
[11] M. R. Weismiller, J. Y. Malchi, R. A. Yetter, T. J. Foley Dependence of Flame Propagation on Pressure and Pressurizing Gas for an Al/CuO Nanoscale Thermite, *Proc. Combust. Inst.* **2009**, *32*, 1895–1903.
[12] G. V. Ivanov, V. G. Surkov, A. M. Viktorenko, A. A. Reshetov, V. G. Ivanov, Anomalous Dependence of the Combustion Rate of Thermite Mixtures on the Pressure, *Combust. Explos. Shock Waves (Engl. Transl.)* **1979**, *15*, 266 – 268.
[13] Yajing Peng, Yinghui Wang, B. Palpant, Xing He, Xianxu Zheng, Yanqiang Yang, Modeling Heat-induced Chemical Reaction in Nanothermites Excited by Pulse Laser: A Hot-Spot-Model, *Int. J. Modern Phys. B* **2010**, *24*, 381–395.
[14] S. Kelzenberg, V. Weiser, E. Roth, N. Eisenreich, B. Berger, B. Haas, Hot Spot Modeling of Thermite Type Reactions Regarding Particle Size and Composition; *EuroPyro 2007 (9ième Congrès International de Pyrotechnie du GPTS) and the 34th International Pyrotechnics Seminar*, Beaune, France, October 8–11, **2007**, Proceedings by GTPS (Groupe de Travail de Pyrotechnie, France and the International Pyrotechnics Society, **2007**, vol. 1, pages 81–796.
[15] V. Weiser, S. Kelzenberg, N. Eisenreich, Influence of Metal Particle Size on the Ignition of Energetic Materials, *Propellants Explos. Pyrotech.* **2001**, *26*, 284 – 289.
[16] G. Langer, N. Eisenreich, Hot Spots in Energetic Materials, *Propellants Explos. Pyrotech.* **1999**, *24*, 113 – 118.
[17] N. Eisenreich, T. S. Fischer, G. Langer, S. Kelzenberg, V. Weiser, Burn Rate Models for Gun Propellants, *Propellants Explos. Pyrotech.* **2002**, *27*, 142 – 149.
[18] H. S. Carslaw, J. C. Jaeger, *Conduction of Heat in Solids*, 2nd ed., Clarendon Press, Oxford, UK, **1973**.
[19] W. H. Press, B. P. Flannery, S. A. Teukolsky, W. T. Vetterling, *Numerical Recipes*, Cambridge University Press, London, UK, **1986**.
[20] B. Noläng, *Ekvi System 3.2*, BeN Systems, Balinge, Sweden, **2004**.
[21] V. Weiser, H. Ebeling, M. Weindel, W. Eckl, T. Klahn, Non-intrusive Burning Rate Measurement under Pressure by Evaluation of Video Data, *35th International Annual Conference of ICT*, Karlsruhe, Germany, June 29–July 2, **2004**, pp. 158-(1–6).
[22] V. Weiser, N. Eisenreich, Fast Emission Spectroscopy for a Better Understanding of Pyrotechnic Combustion Behaviour, *Propellants Explos. Pyrotech.* **2005**, *30*, 67 – 78.
[23] *CRC Handbook of Chemistry and Physics* (Ed.: D. R. Lide), 72nd ed., CRC Press, Boca Raton, FL, USA, **1992**.
[24] N. Eisenreich, Direct Least Squares Fit of Chemical Reaction Curves and its Relation to the Kinetic Compensation Effect, *J. Therm. Anal.* **1980**, *19*, 289 – 296.
[25] S. M. Umbrajkar, M. Schoenitz, E. L. Dreizin, Exothermic Reactions in Al-CuO Nanocomposites, *Thermochim. Acta* **2006**, *451*, 34 – 43.
[26] Xiaoning Wen, D. E. Hare, and D. D. Dlott, Laser Polymer Ablation Threshold lowered by Nanometer Hot Spots, *Appl. Phys. Lett.* **1994**, *64*, 184.
[27] S. H. Fischer, M. C. Grubelich, A Survey of Combustible Metals, Thermites, and Intermetallics for Pyrotechnic Applications, *32nd AIAA/ASME/SAE/ASEE Joint Propulsion Conference*, Lake Buena Vista, FL, USA, July1–3, **1996**, AAIA paper 96–3018.

Received: January 20, 2014
Revised: April 9, 2014

